Analogue modelling of fault reactivation: tectonic inversion and oblique remobilisation of grabens

Agnès Dubois[a,*], Francis Odonne[b], Gérard Massonnat[c], Thomas Lebourg[d], Richard Fabre[d]

[a]*U.M.R. 5 563, C.N.R.S., Université Paul Sabatier, Toulouse, France*
[b]*Laboratoire de Dynamique des Bassins Sédimentaires, Université Paul Sabatier, Toulouse, France*
[c]*Elf Aquitaine, Exploration—Production, Pau, France*
[d]*Centre de développement des geosciences appliquées, Université de Bordeaux I, France*

Abstract

Analogue models of sand above a silicone layer were examined to determine the effects of normal fault reactivation. Models were first subjected to extension, which lead to the formation of two linear grabens. Each model was then subjected to a second phase deformation, either parallel or oblique to the previous initial extension, and either extensional or contractional. The influence of sedimentation has been evaluated using experiments with and without sedimentation. In cases of oblique secondary deformation, all newly formed faults were parallel to the older grabens, thus they were oblique to the direction of the principal stress directions during the second deformation phase. In experiments without sedimentation, all older faults were reactivated, whereas in experiments with sedimentation, some of the older faults were not reactivated. In the case of an oblique compressional secondary deformation phase with post rift sedimentation, strain partitioning occurred between reactivated older normal faults and new reverse faults. σ_2 was vertical on reactivated normal fault planes, whereas σ_3 was vertical on reverse fault planes. In the case of oblique compressional secondary deformation phase without post rift sedimentation, no strain partitioning was observed. In this model, σ_3 was vertical on every fault plane. It is therefore concluded that sedimentation within grabens induces a variation of stress orientation and strain partitioning. © 2002 Elsevier Science Ltd. All rights reserved.

Keywords: Analogue modelling; Tectonic inversion; Linear grabens

1. Introduction

When an analogue experiment comprising brittle and viscous layers is submitted to an oblique extension, an 'en échelon' fault system forms (Tron and Brun, 1991; McClay and White, 1995), whereas if the oblique deformation is compressional, the newly formed system is composed of strike-slip faults associated with reverse faults (Richard and Cobbold, 1990; Brun and Nalpas, 1996). If a previous fault set is present in the experiment, fault reactivation, rather than creation of new faults, is frequently observed. Fault reactivation can occur under stress levels lower than those needed for creating new faults (Handin, 1969; Krantz, 1991) because pre-existing faults are surfaces along which the cohesive strength and the friction coefficient are lower than those of intact rocks (Anderson, 1951). Analogue coaxial experiments of tectonic inversions, where the direction of imposed displacement is parallel to that of the early phase, have already been reported (Eisenstadt and Withjack,

1995; Faccenna et al., 1995), whereas only a few experiments of oblique fault reactivation have been performed (Brun and Nalpas, 1996; Keep and McClay, 1997). In nature, only a few sets of faults have been described as being the result of oblique reactivations: the Central Graben of the North Sea (Bartholomew et al., 1993), the northern and southern North Sea (Oudmayer and Dejager, 1993; Faerseth, 1996), the Mohns ridge (Dauteil and Brun, 1993) and the Broad Fourteens basin (Brun and Nalpas, 1996).

We have chosen analogue sand–silicone experiments to study how normal faults could be reactivated during subsequent coaxial or oblique deformation. Brittle sand layers over a soft silicone layer is considered to be a good analogue of sedimentary rocks over evaporites (Richard and Cobbold, 1990; Vendeville and Jackson, 1992). Each experiment involved two successive phases of deformation. During the first phase, a set of two grabens was formed by extension. This set was submitted to a new deformation during the second phase. The new state of stress was either coaxial or oblique (60°) to the first state of stress, and involved either extension or contraction. The influence of sedimentation was

---

* Corresponding author.
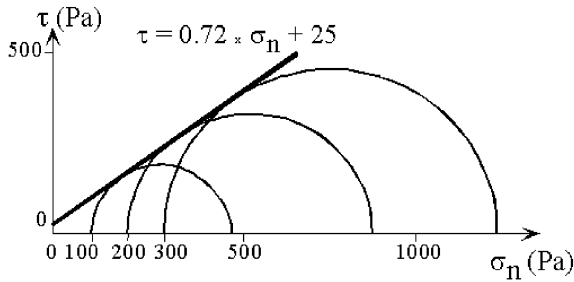 *E-mail address:* agnes.dubois@voila.fr (A. Dubois).

Fig. 1. Mohr diagram illustrating result for triaxial tests performed on dry Fontainebleau sand (300 μm) used in the experiments.

checked by comparing experiments with and without post rift sedimentation. At the end of the deformation, the orientation and dip of the younger faults are good indications of the anisotropy created by the first set of normal faults. Furthermore, passive markers in analogue experiments allow the determination of both dip-slip and strike-slip components of displacement and indicate accurate slip mechanisms on faults.

2. Description of experiment

2.1. Scaling

Analogue models are constructed in the laboratory in an attempt to reproduce, at a smaller scale, structures analogous to those observed in natural systems. Meaningful analogue modelling lies in the proper scaling of model parameters (Hubbert, 1937). Hubbert (1937) established scaling relationships between nature and analogue models demonstrating that dynamic similarity is required to account for the rheological behaviour of the materials. This means that all forces, stresses and linear dimensions must be proportional between nature and model. The geological object we want to model is considered as static or slowly moving; acceleration and hence the force due to inertia is therefore nearly zero. Therefore, only gravity forces remain (Hubbert, 1937; Davy and Cobbold, 1988). In the following, 'nature' refers to the natural object whose properties will be scaled down to design the analogue model.

Let Φ (Eq. (1)) be the force ratio, μ the mass ratio, γ the acceleration ratio, λ the length ratio and τ the time ratio.

$$\Phi = \mu\gamma = \mu\lambda\tau^{-2} \qquad (1)$$

Dynamic similarity is satisfied when μ, λ and τ are independently chosen one apart from the other, and when the sum of all forces satisfies $\Phi = \mu\lambda_{\text{gravity}} = \mu$ (Hubbert, 1937).

Practical constraints of space and time span to run experiments in the laboratory imposed length and time ratios. In our model where sedimentary cover of 5 km is modelled by a sand layer of 5 cm thickness, and deformation of 1 Ma in nature is modelled in 1 h in the laboratory, the length and

time ratios between experiment and nature are $\lambda = 10^{-5}$ and $\tau = 10^{-10}$.

Natural salt is assumed to have a newtonian behaviour (Weijermars et al., 1993). So, analogue modelling of salt deformation needs to consider the velocity ratio, V, and the density contrast with sediment cover and viscosity ratio, η. Let D be the density ratio, then

$$V = \lambda\tau^{-1} = 10^5 \qquad (2)$$

and

$$\eta = D\lambda\tau \qquad (3)$$

λ and τ are imposed by the requirements in the laboratory. Eqs. (2) and (3) impose density, viscosity and displacement rate ratios. Density and viscosity ratios restrict the choice of material that could be used in the analogue model. The volumetric mass of salt is 2.2×10^3 kg m^{-3} and its viscosity is 10^{18} Pa s (Cobbold et al., 1986; Vendeville and Jackson, 1992; Carter et al., 1993; Weijermars et al., 1993). Considering the density ratio between salt and sediment, the viscosity of the salt layer and Eq. (3), dynamic similarity leads to an analogue material that should have a density around 1.27×10^3 kg m^{-3} and a viscosity around 10^3 Pa s. Silbione Putty (gomme 7009), usually called silicone, manufactured by Rhône–Poulenc, has a viscous behaviour (Weijermars, 1986) and possesses physical properties as cited above (Cobbold et al., 1989). Thus, silicone was selected as an analogue of salt in the present models. We performed in the laboratory experiments at 2.5 cm h^{-1}. This displacement rate represents in nature a displacement rate of 0.25 cm year^{-1} (Eq. (2)). Considering that rates of a few cm year^{-1} are the rates of tectonic plates and that tens of faults and grabens accommodate that deformation in the North Sea, an extensional rate of 0.25 cm year^{-1} for simulating only two grabens is reasonable.

Natural sediments are assumed to have a Coulomb behaviour (Byerlee, 1978). The deformation of the sedimentary cover is modelled by dry, pure quartz sand from Fontainebleau (France). Sand is an analogue material that has been widely used (Hubbert, 1951; Cobbold et al., 1989; McClay and White, 1995; Brun and Nalpas, 1996; Keep and McClay, 1997). Dry quartz sand is a frictional plastic material that deforms by slip along fault surfaces or narrow dilating shear zones (Mandl et al., 1977; Desrues, 1985; Mandl, 1988; Krantz, 1991). The angle of internal friction of sediments is between 30° (for 2×10^2 MPa $< \sigma_n < 20 \times 10^2$ MPa) and 40° (for $\sigma_n < 2 \times 10^2$ MPa); and cohesion is between 0 and 60 MPa (Byerlee, 1978; Brace and Kohlstedt, 1980). Deformation tests performed on Fontainebleau sand in a triaxial deformation press show an angle of internal friction of 35°, and a very low cohesion of about 15 and 25×10^3 Pa (Fig. 1). That is very close to what is considered to represent the brittle behaviour of the upper crust (Byerlee, 1978). Compaction effects in the model can be neglected if the sand thickness is less than 15 cm (Davidson et al., 1993).
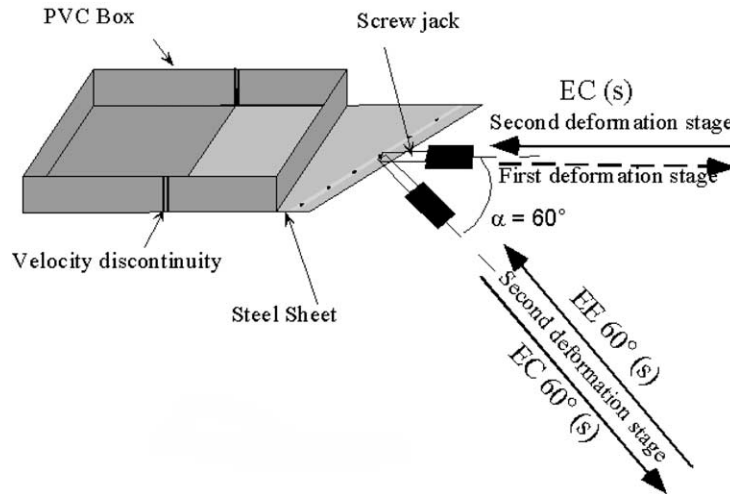
Fig. 2. Deformation apparatus used in the present experiments. The size of the PVC box is $50 \times 60 \times 10$ cm^3, and it is driven by a computer-controlled stepper motor. The steel sheet creates a velocity discontinuity at the box centre during deformation. E refers to an extensional deformation. C refers to a compressional deformation. s refers to post-rift sedimentation after the first deformation stage.

2.2. Deformation apparatus and method

Experiments were performed using a $50 \times 60 \times 10$ cm^3 PVC box (Fig. 2). A steel sheet of 0.5 mm thickness creates a velocity discontinuity at the centre of the box. The steel sheet is fixed to a screw jack operated by a computer-controlled stepper motor, which allows precise control of displacement and strain rate.

All our models are made of silicone and a sand layer of 5 cm thickness. The silicone layer was constrained to the central part of the experiment, which coincided with the position of the displacement discontinuity. Dimensions of the silicone layer were $60 \times 15 \times 1.7$ cm^3. Coloured sand was sieved over the silicone in the box. Photographs of the top of the model were taken all along the deformation process. In the deformed model, vertical sections were made perpendicular to the velocity discontinuity. Based on these recordings, the three-dimensional shape of the model can be reconstructed.

2.3. First extensional deformation phase

The same extensional deformation was first imposed on each model. The extension direction was perpendicular to the velocity discontinuity, and the bulk displacement was limited to 2.5 cm for all experiments. After the first deformation phase, two parallel grabens appear, one on each side of the velocity discontinuity. A reference experiment was stopped after this single extension phase; the section provides data on the geometry of the first set of faults. We measured after 2.5 cm displacement (16.7% of strain) that grabens are 4.4 cm wide (mean calculated on 21 sections in the same model, standard deviation is 0.2) and separated by 10.1 cm (mean calculated on 21 sections in the same model, standard deviation is 0.5). Dips of grabens bounding faults are between 56 and 65°. The faults that bound the grabens had quite planar shapes and had strike parallel to the velocity discontinuity.
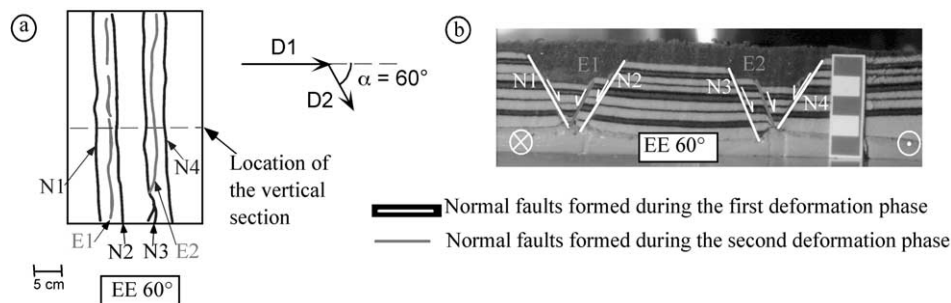

Fig. 3. Display of analogue model EE 60° in map (a) and cross-section (b). These figures illustrate the situation after the first extensive deformation, 2.5 cm, followed by an oblique extensional secondary phase, 1.25 cm. Scale is in centimetres. (a) Map view: master faults N1, N2, N3 and N4 define the first graben set. Passive markers indicate the strike-slip displacements during the second phase. Faults (E1 and E2) associated with the second extensional phase are parallel to grabens of the first extension phase although σ_3 is oriented 60° to that of the first phase. (b) Cross-section: arrows indicate slip during the second tectonic phase. Offsets of black and grey layers indicate the whole dip-slip displacements during the two deformation phases. All faults formed during the first extensive phase (N1, N2, N3 and N4) are reactivated in normal mode.
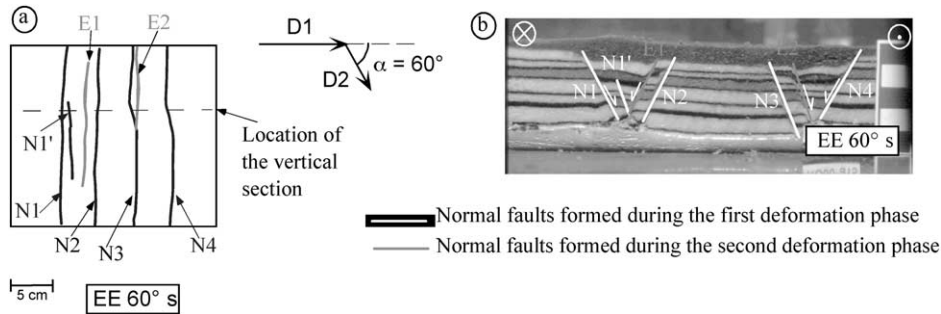
Fig. 4. Display of analogue model EE 60°s in map (a) and cross-section (b). These figures illustrate the situation after the first extensional deformation, 2.5 cm, and post rift sedimentation, followed by an oblique extensive secondary phase, 1.25 cm. Scale is in centimetres. (a) Map view: master faults N1, N2, N3 and N4 define the first grabens set. Passive markers highlight the strike slip displacement during the secondary phase. Faults (E1 and E2) associated with the second extensional phase are parallel to grabens of the first extension phase although σ_3 is oriented 60° to that of the first phase. (b) Cross-section: arrows indicate slip during the secondary tectonic phase. Offsets of black and grey layers indicate the dip-slip displacement during each phase of deformation. N1 and N4 were reactivated. Three faults (N1′, N2 and N3) were not reactivated unlike experiment EE 60° without sedimentation.

2.4. Second deformation phase

In all other experiments, the first fault set was subjected to a second deformation phase. This new deformation was either coaxial or obliquely (60°) oriented compared with the first direction, and either extensional or compressional. The first two models were performed under oblique extension (1.25 cm, experiments EE 60° and EE 60°s; Figs. 3 and 4), the next two models were shortened by 2.5 cm coaxially (EC and ECs; Figs. 5 and 6), and the last two models were shortened by 5 cm obliquely (EC 60° and EC 60°s; Figs. 7 and 8); see also Table 1. Dip-slip components were measured in cross-sections, and strike-slip components were measured in plan view photos. The influence of sedimentation was evaluated in some experiments by filling the

grabens with sand before the second deformation phase. Experiments with sedimentation between the two deformation phases allow us to distinguish the component of dip-slip produced during the first tectonic phase from that produced during the second phase. The thickness of the post-first phase sedimentation gives a measurement of the dip-slip that was produced during the primary phase. As experiments carried out without sedimentation do not give information on dip-slip during the primary extensional deformation, we assume that this dip-slip during the primary tectonic phase measured in the case of experiments with sedimentation is the same for experiments without sedimentation. All measurements of both dip-slip and strike-slip are given in Table 2. It was possible to calculate dip-slip for 11 and strike-slip for six cases.
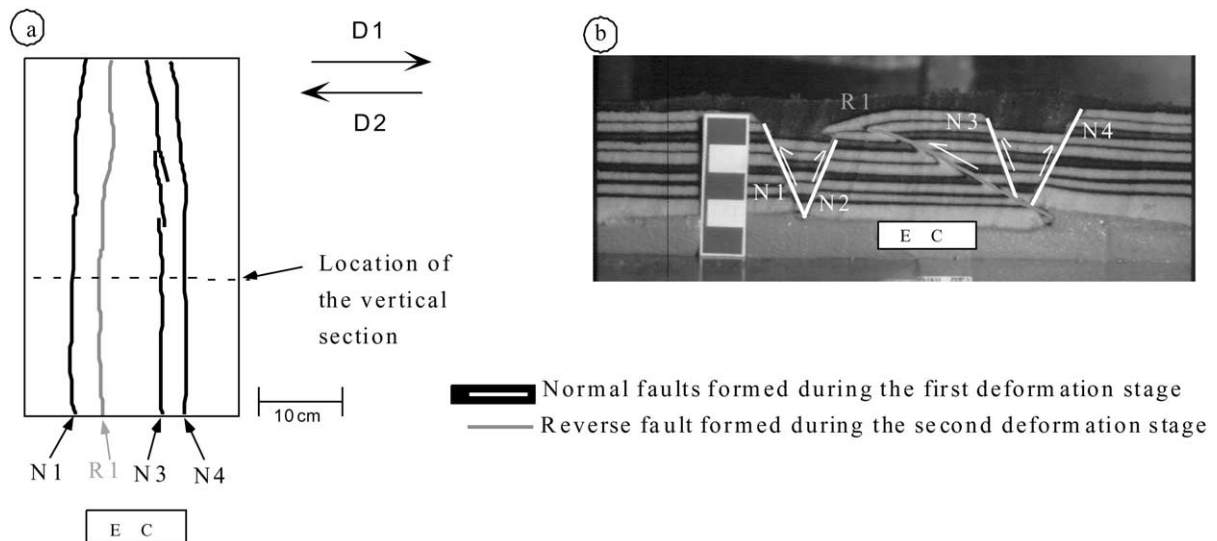

Fig. 5. Display of analogue model EC in map (a) and cross-section (b). These figures illustrate the situation after the first extensional deformation, 2.5 cm, followed by a shortening secondary stage, 2.5 cm. Scale is in centimetres. (a) Map view: master faults N1, N2, N3 and N4 define the first graben set. A reverse fault (R1), associated with the second shortening phase, is formed parallel to the grabens. (b) Cross-section: arrows indicate slip during the secondary tectonic phase. Offsets of black and grey layers indicate the whole dip-slip displacements during the two deformation phases. All faults formed during the first extensive phase (N1, N2, N3 and N4) are reactivated in reverse mode.
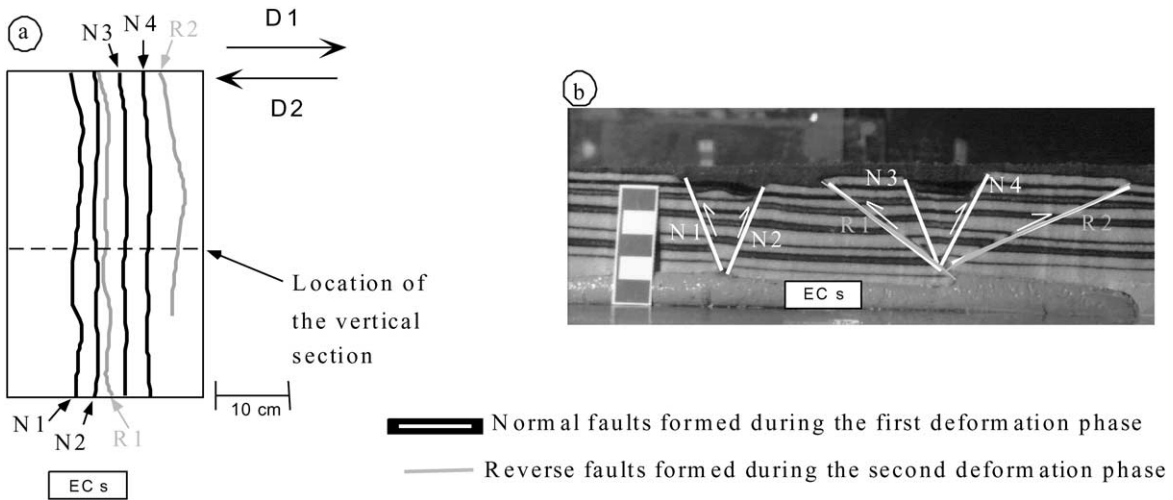
Fig. 6. Display of analogue model ECs in map (a) and cross-section (b). These figures illustrate the situation after the first extensional deformation, 2.5 cm, and post rift sedimentation followed by a second shortening phase, 2.5 cm. Scale is in centimetres. (a) Map view: master faults N1, N2, N3 and N4 define the first graben set. Reverse faults (R1 and R2), associated with the second shortening phase, formed parallel to grabens. (b) Cross-section: arrows indicate slip during the second tectonic phase. Offsets of black and grey layers indicate the dip-slip displacements during each phase of deformation. N1, N2 and N4 are reactivated in reverse mode. One fault (N3) is not reactivated unlike experiment EC without sedimentation.

3. Results

For all experiments described below, the first deformation phase was extensional and E refers to an extensional deformation, C to a compressional deformation and s to a sedimentation stage between the two successive phases. On all the sections, the fault formed during the first extensional phase are indicated as 'N' faults (N1, N2,...). Three different features have been investigated.

3.1. Extension followed by oblique extension

Here, two experiments are presented: EE 60° without sedimentation and EE 60°s with sedimentation after the first extensional phase. In both experiments the first extensional phase was followed by a second extensional phase with extension direction oriented 60° to that of the first phase.

In experiment EE 60°, no sedimentation occurred (Fig. 3). During the second phase of deformation, two
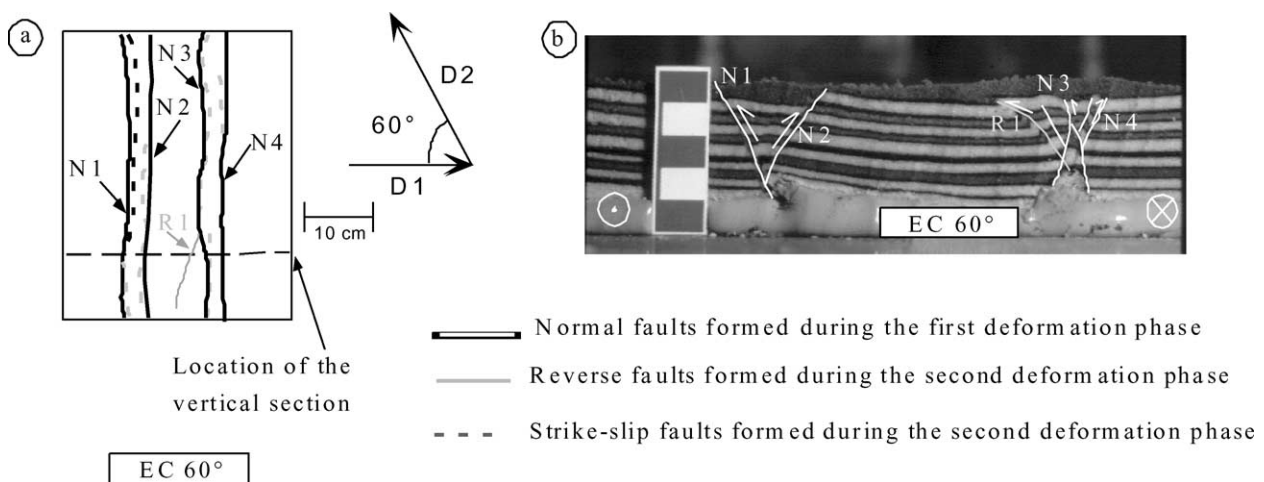

Fig. 7. Display of analogue model EC 60° in map (a) and cross-section (b). These figures illustrate the situation after the first extensional deformation, 2.5 cm, followed by an oblique second shortening phase, 5 cm. Scale is in centimetres. (a) Map view: master faults N1, N2, N3 and N4 define the first graben set. Passive markers indicate the strike-slip displacement during second phase. Fault (R1) associated with the second shortening phase is parallel to grabens of the first extension phase although σ_1 is oriented 60° to σ_3 of the first phase. (b) Cross-section: arrows indicate slip during the secondary tectonic phase. Offsets of black and grey layers indicate the whole dip-slip displacements during the two deformation phases. All faults formed during the first extensive phase (N1, N2, N3 and N4) are reactivated in reverse mode.
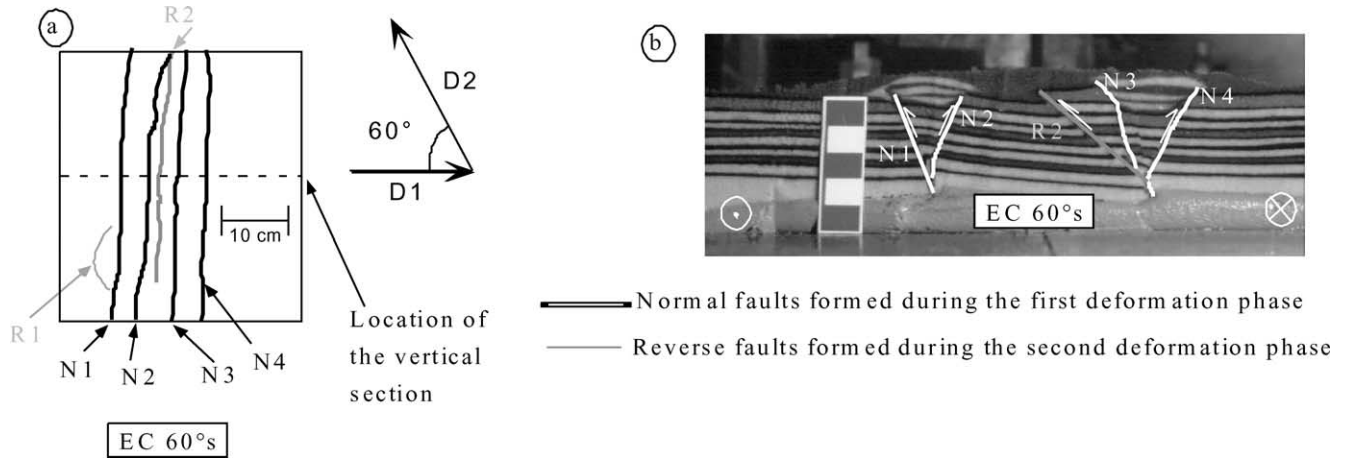
Fig. 8. Display of analogue model EC 60°s in map (a) and cross-section (b). These figures illustrate the situation after the first extensional deformation, 2.5 cm, and post rift sedimentation, followed by an oblique second shortening phase, 5 cm. Scale is in centimetres. (a) Map view: master faults N1, N2, N3 and N4 define the first graben set. Passive markers indicate the strike-slip displacement during the second phase. Faults (R1 and R2) associated with the second shortening phase are parallel to grabens of the first extension phase although σ_1 is oriented 60° to σ_3 of the first phase. (b) Cross-section: arrows indicate slip during the second tectonic phase. Offsets of black and grey layers indicate the dip-slip displacement during each phases of deformation. N1, N2 and N4 are reactivated in reverse mode. One fault (N3) is not reactivated unlike experiment EC 60° without sedimentation.

new normal faults (E1 and E2) were formed. They were located inside the former grabens and oriented parallel to them. E1 dipped 64° and E2 68°. It was not possible to separate strike-slip on N2–N3 from E1–E2 because of the small amount of displacement. All faults formed during the first tectonic phase were reactivated during the oblique extensional phase.

In experiment EE 60°s, sedimentation occurred between the two phases of deformation (Fig. 4). During the second phase of deformation, two new normal faults (E1 and E2) were formed. They were located inside and parallel to the former grabens, that is to say oblique to the extension direction of the second phase. The dips of these faults were, respectively, 63 and 70°. Two faults (N2 and N3), formed during the first tectonic phase, were not reactivated during the second one but their dip steepened to 64° in both cases. The steepening is inferred from the comparison between dips of faults of the reference experiment and dips of faults of experiment EE 60°s. The two other faults (N1 and N4) formed during the first tectonic phase were reactivated in normal mode and their dips steepened by approximately 5° for both.

3.2. Extension followed by coaxial shortening

Here, two experiments are presented: EC without sedimentation and ECs with sedimentation after the first extensional phase. In both experiments the first extensional phase was followed by a coaxial compressional second phase.

In experiment EC (Fig. 5), during the second phase of deformation, one reverse fault (R1) was created between the two grabens and parallel to them. Its dip was 25°. All faults formed during the first tectonic phase were reactivated in the reverse mode, and their dips were steepened at an average of 10°. The steepening could result from horizontal compaction during shortening.

In experiment ECs, post-rift sedimentation occurred (Fig. 6). During the second phase of deformation, two reverse faults (R1 and R2) were created, one between the two grabens and one outside, but both parallel to them with dips between 27 and 34°. They are antithetic and form a pop-up that ejects one of the grabens. One fault (N3), formed during the first phase of deformation, was not reactivated during the second deformation phase. This fault plane became steepened by 68° from 60°. All other faults

Table 1
Experimental parameters used in the present experiment. α is the angle between the first phase extensional axis and the second phase extension axis, or shortening axes. 'Sedimentation' refers to post rift sedimentation (or not) in grabens after the first deformation phase

First deformation phase	Second deformation phase	α (°)	Sedimentation	References	Figure
Extension of 2.5 cm.	Extension of 1.25 cm.	60	No	EE 60	3
			Yes	EE 60 s	4
	Compression of 2.5 cm.	0	No	EC	5
			Yes	EC s	6
	Compression of 5 cm.	60	No	EC 60	7
			Yes	EC 60 s	8

Table 2
Parameters are recorded at the end of the first tectonic phase. 'Dip-slips' are mean values calculated from 11 dip-slip measurements. 'Strike-slips' are mean values calculated from six strike-slip measurements. Standard deviations are given in brackets. *r* refers to a reverse dip-slip

	Faults	First tectonic phase	Second tectonic phase		
		Dip-slip (cm)	Dip (°)	Dip-slip (cm)	Strike-slip (cm)
EE 60 (Fig. 3)	N1	0.89 (0.14)	59.4	0.68 (0.09)	0.3 (0.10)
	E1 + N2	0.76 (0.13) N2	63.7 + 60.3	0.53 (0.05)	0.19 (0.06)
	N3 + E2	0.49 (0.04) N3	68 + 67.9	0.48 (0.09)	0.19 (0.05)
	N4	0.94 (0.10)	61.4	0.76 (0.12)	0.27 (0.09)
EC (Fig. 5)	N1	1.27 (0.11)	63.5	0.22-r (0.04)	
	N2	0.86 (0.07)	67.9	0.04-r (0.03)	
	R1	0	25	1.14-r (0.06)	
	N3	0.95 (0.15)	71.2	0.3-r (0.09)	
	N4	1.29 (0.12)	62.2	0.25-r (0.02)	
EC 60 (Fig. 7)	N1	1.03 (0.15)	67.5	0.808-r (0.12)	1.72 (0.10)
	N2	1.09 (0.12)	63.2	0.68-r (0.12)	0.38 (0.18)
	R1	0	40.5	0.37-r (0.03)	0.45 (0.03)
	N3	1.05 (0.08)	68	0.88-r (0.34)	0.65 (0.30)
	N4	1.35 (0.11)	69.1	1.34-r (0.30)	1.37 (0.47)
EE 60s (Fig. 4)	N1 + N1′	0.89 (0.14)	59.5 + 60.1	0.64 (0.13)	0.45 (0.09)
	E1	0	62.8	0.43 (0.06)	0.3 (0.05)
	N2	0.76 (0.13)	66.6	0	0
	N3	0.49 (0.04)	63.7	0	0
	E2	0	69.4	0.34 (0.06)	0.2 (0.05)
	N4	0.94 (0.10)	57.2	0.71 (0.06)	0.625 (0.16)
EC s (Fig. 6)	N1	1.25 (0.11)	65.8	0.14-r (0.08)	
	N2	0.87 (0.07)	67.2	0.14-r (0.09)	
	R1	0	34.1	1-r (0.04)	
	N3	0.96 (0.15)	68.7	0	
	N4	1.28 (0.12)	63.5	0.11-r (0.03)	
	R2	0	27.5	0.24-r (0.02)	
EC 60 s (Fig. 8)	R1	0	40.2	0.46-r (0.03)	0.73 (0.16)
	N1	1.025 (0.15)	68.4	0.558-r (0.23)	1.6 (0.44)
	N2	1.075 (0.12)	65.9	0.455-r (0.13)	1.04 (0.74)
	R2	0	42	0.688-r (0.06)	1.01 (0.10)
	N3	1 (0.08)	76.7	0	0
	N4	1.446 (0.11)	61	0.405-r (0.14)	1.1 (0.27)

formed during the first phase were reactivated in the reverse mode and the dip angles were steepened by 5°. The steepening is inferred from the comparison between dips of faults of the reference experiment and dips of faults of experiment ECs.

3.3. Extension followed by oblique shortening

Here, two experiments are presented: EC 60° without sedimentation and EC 60°s with sedimentation after the first extensional phase. In both experiments the first extensional phase was followed by a second compressional second phase with compression direction oriented 60° with respect to the extension direction of the first phase.

In experiment EC 60° (Fig. 7), an apparent flower structure was observed in the right part of the model. One reverse fault (R1), rooted at the bottom of one of the grabens, was propagated between grabens and formed parallel to the first generation faults. This reverse fault has a high dip value: 40° (measured in the middle of the fault plane). Four strike-slip faults formed parallel and very close to the graben bounders.

Those strike-slip faults were located so close to graben bounders that it was very difficult to distinguish them from the graben bounding faults. In the following discussion, we consider that they are making one single structure, and that the former faults (N1, N2, N3 and N4) are reactivated during the second phase of deformation. So, we concluded that all faults formed during the first tectonic phase were reactivated, and their average dips were steepened to 63°.

In experiment EC 60°s sedimentation occurred between the two phases of deformation (Fig. 8). Two reverse faults (R1 and R2), parallel to grabens and located at the left of each graben were formed. Their dips lie between 40 and 42°. One fault (N3), which formed during the first tectonic phase, was not reactivated during the second phase, but its dip angle was clearly steepened from 60° up to 76°. All other faults were reactivated as reverse faults and dips of fault planes were steepened by 10°.

In summary of the results from the present experiments, the second phase of deformation induced a steepening of faults when the secondary stress state was compressive and
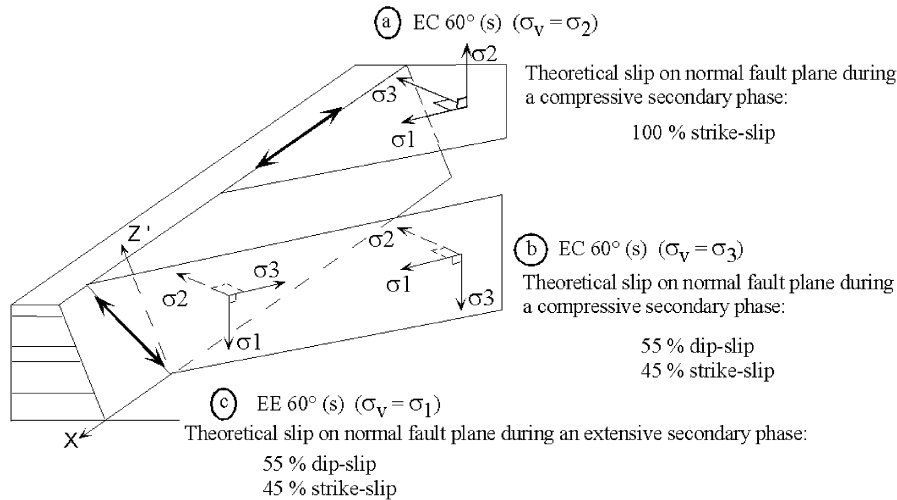
Fig. 9. Representation of the intersection of the fault plane with the second phase stress vector plane ($\sigma_1-\sigma_3$). One stress orientation is allowed for an extensional second deformation phase: σ_1 must be vertical. Two stress orientations are allowed for a compressive secondary deformation phase: σ_2 or σ_3 may be vertical. The projection of the second phase stress vector on the reverse fault plane gives the relative magnitude of dip-slip compared with strike-slip.

when the secondary stress state was extensive in the experiment with sedimentation (EE 60° s). It is also noted that almost all external primary normal faults bounding the area of deformation and new reverse faults accommodated most of the deformation. In experiments with sedimentation, six second phase faults formed while most first phase faults were reactivated. For the opposite, in experiments without sedimentation, only four second phase faults formed and all first phase faults were reactivated. In all cases, secondary phase faults formed under an oblique secondary tectonic stress state were parallel to the first phase normal faults. In other words, all new faults were oriented obliquely to the secondary direction of extension or contraction.

3.4. Analysis of dip-slip versus strike-slip components during reactivation

Following Anderson (1951), the active displacement vector on a fault plane is defined as a line being the intersection of the fault plane itself and the ($\sigma_1-\sigma_3$) plane of the applied stress state. This active displacement vector can be divided into dip-slip and strike-slip components on the fault plane. In our experiments a theoretical displacement vector can be expected as being the intersection of the fault plane

and the ($\sigma_1-\sigma_3$) plane of the applied stress state. This theoretical vector is often named in the following as the 'optimal slip'. Let us consider in Figs. 9 and 10 some examples.

In Fig. 9, a first phase normal fault is reactivated under an oblique compressive second phase. In the case of a compressional secondary phase (EC60° and EC 60°s), σ_1 is horizontal. σ_2 and σ_3 may be either vertical or horizontal. In the case where σ_2 is vertical, the ($\sigma_1-\sigma_3$) plane is horizontal and the optimal slip will be a pure strike-slip vector parallel to the first phase fault. In the case where σ_3 is vertical, the ($\sigma_1-\sigma_3$) plane is vertical and the optimal slip on the fault plane can be divided into two components: 55% dip-slip and 45% strike-slip.

In the case of an extensional secondary phase (EE 60° and EE 60° s), σ_1 is vertical and σ_3 is horizontal; as a result the ($\sigma_1-\sigma_3$) plane is vertical. In this case, the direction of the vector is opposite that of the previous example but the theoretical relative magnitudes of dip-slip and strike-slip for a normal fault are unchanged, that is to say, 55% dip-slip and 45% strike-slip (Fig. 9c).

In Fig. 10, we represent the relative magnitude of dip-slip and strike-slip on a reverse fault during a contractional oblique secondary tectonic phase (EC 60° and EC 60°s). The only stress orientation allowed is σ_1 horizontal with σ_3 vertical. The theoretical relative magnitude of dip-slip
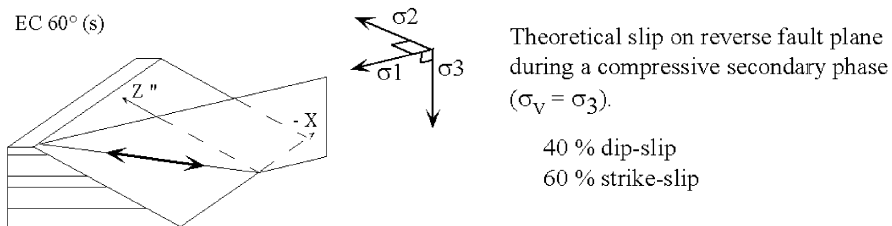

Fig. 10. Representation of the intersection of a reverse fault plane with the second phase stress vector plane ($\sigma_1-\sigma_3$). Only one stress orientation is allowed: σ_3 must be vertical. The projection of the second phase stress vector on the reverse fault plane gives the relative magnitude of dip-slip compared with strike-slip.
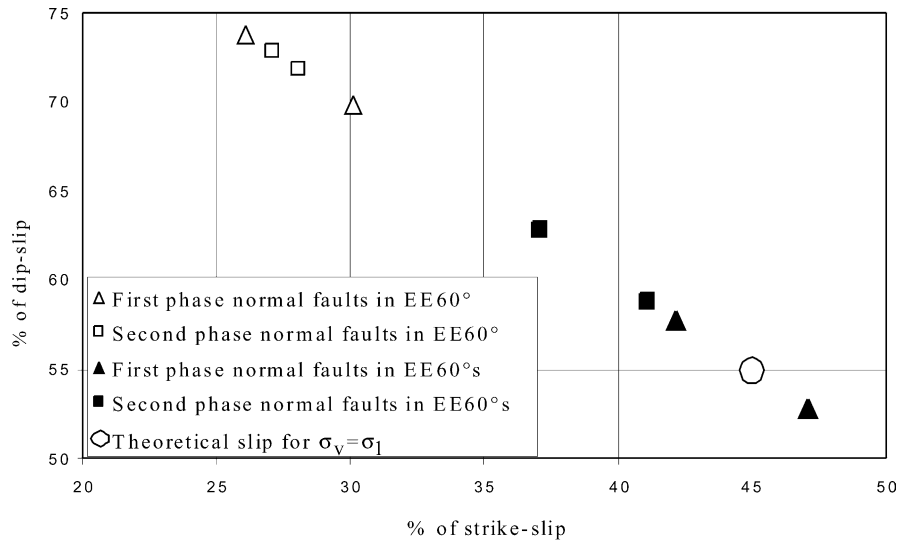
Fig. 11. Relative magnitude of dip-slip component compared with strike-slip component on normal faultplanes in experiments with an oblique and extensional second deformation phase. Dip-slip magnitude is more important in experiments without sedimentation than experiments with. Slip on fault planes in experiments carried with sedimentation tends to fit the theoretical slip.

and strike-slip for a reverse fault is 40% dip-slip and 60% strike-slip.

In our experiments, dip-slip and strike-slip components were measured on each fault at the end of the second deformation phase. Then, the final vector (strike-slip, dip-slip) was calculated (Table 2). Figs. 11 and 12 show a comparison of the calculated theoretical vectors (see

Figs. 9 and 10) and the final vectors measured in the experiments.

In Fig. 11 we represent the percentage of observed dip-slip as a function of observed strike-slip on normal faults that experienced oblique extensional second phase deformation. A point located at 45% strike-slip and 55% dip-slip indicates the theoretical optimal slip. Oblique slip refers to
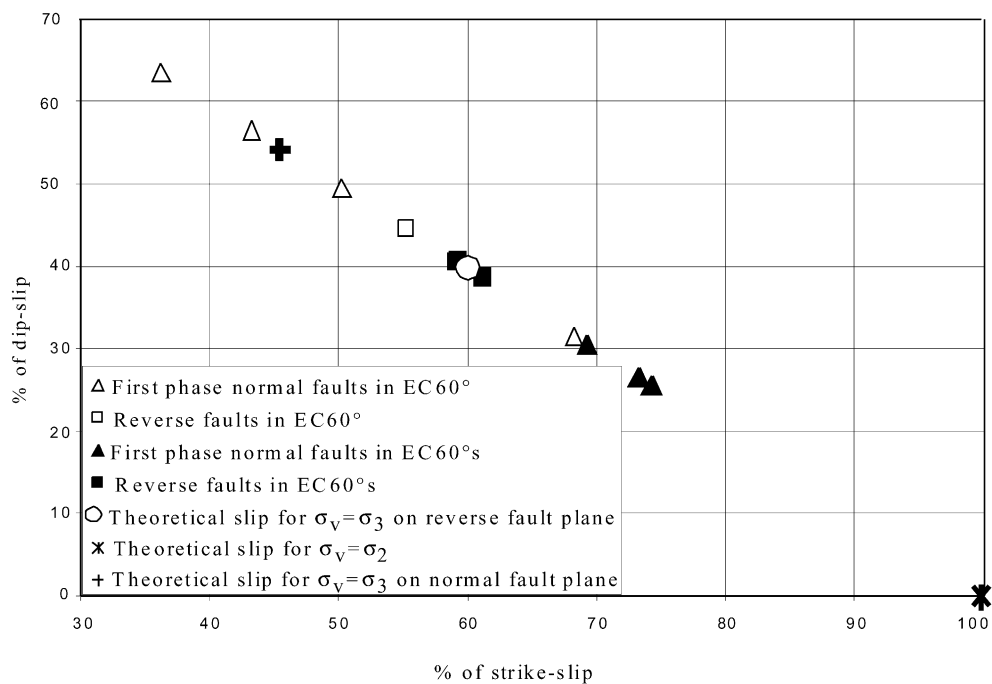

Fig. 12. Relative magnitude of dip-slip compared with strike-slip component on both normal and reverse faults in experiments with an oblique shortening second deformation phase. Reverse faults tend to fit theoretical slip in the case of σ_3 being vertical. Experiments carried without sedimentation have slip on normal fault planes close to theoretical slip for σ_3 being vertical. In experiments carried with sedimentation, slip on normal fault planes tends to fit the theoretical slip for σ_2 being vertical.

the combination of both dip slip and strike slip. All faults show oblique slip with a dip-slip component greater than 50%. In EE60°, the mean oblique-slip component is 28% strike-slip for 72% dip-slip, and in EE60°s, the mean oblique-slip component is 42% strike-slip for 58% dip-slip. The oblique slip observed on most normal faults has a dip-slip component greater than the theoretical value. Grabens filled with sediments (in the EE 60°s experiment) have a strike-slip component of displacement greater than grabens without. They better fit the theoretical relative magnitude of dip-slip and strike-slip direction. On the other hand, grabens that are not filled with sediments have greater dip-slip components. Sedimentation balances deformation on the faults, leading to similar values of dip-slip and strike-slip.

In Fig. 12 we represent the relative magnitude of dip-slip and strike-slip of all faults in experiments where the second deformation phase is oblique and compressive (EC 60° and EC 60°s): 60% strike-slip and 40% dip-slip in the case of a reverse fault (Fig. 10), 100% strike-slip when σ_2 is vertical along a first phase normal fault and 55% of dip-slip and 45% of strike-slip when σ_3 is vertical along a first phase normal fault (Fig. 9). The final vectors measured in the experiments are compared with the calculated theoretical vectors: in EC 60°, the mean oblique slip on the normal fault is 51% strike-slip for 49% dip-slip, which is close to the theoretical relative magnitude of dip-slip and strike-slip in the case where σ_3 is vertical. The R1 reverse fault accommodates 55% strike-slip for 45% dip-slip. In the corresponding experiment with sedimentation (EC60°s), the mean oblique slip on normal fault plane is 72% strike-slip for 28% dip-slip. In this case, slip tends to be partitioned, it gets closer to the theoretical relative magnitude of dip-slip and strike-slip in the case where σ_2 is vertical. The R1 and R2 reverse faults accommodate 60% strike-slip for 40% dip-slip (Table 2), exactly the theoretical relative magnitude of dip-slip and strike-slip expected. From these two experiments, with and without sedimentation, it appears that grabens that have been filled with sediments and reactivated in the oblique reverse mode display a strike-slip component higher than grabens without sediments, implying a stress state when σ_2 is vertical. On the other side, reverse faults in experiments without sedimentation fit with the situation where σ_3 is vertical. The position of σ_2 and σ_3 appears to be switched from grabens to reverse faults and strain is partitioned.

4. Discussion

In the present positive structural inversion experiments, EC(s) and EC 60°(s), where sand and silicone putty have been used, only block tilting without any folding has been observed. Letouzey (1990) showed that before reactivation of faults, flexuring and folding of the sediment cover occurred. This phenomenon is most likely due to the reacti-

vation of the fault at depth and to the prevention of surface movement. In the present experiments the surface was not prevented from strain, and the entire fault was commonly reactivated without any stage of folding.

Richard and Krantz (1991) showed that oblique-slip may be explained by faults that are listric in sections. Here, we observe that oblique slip can occur on analogue planar faults.

Following Huyghe and Mugnier (1992), short-cut geometry is expected on a pre-existing steeply dipping fault when the ratio between the cohesion of the intact rock, and the cohesion on the reactivated fault, C_{of}, is higher than 0.2. In our experiments, where all present pre-existing steeply dipping faults and where the ratio C_o/C_{of} is about 1.02, that is to say clearly higher than 0.2, no short-cut geometry is observed.

Tron and Brun (1991) and McClay and White (1995) showed that intra-rift faults are orthogonal to the tectonic stress in a young lithosphere and that they form an en échelon system when the stress state is oblique to the bounding faults of the rift. They describe an oceanic crust while we model a pre-structured continental crust. This is probably why our results are somewhat different. Experiments EE60° and EE60°s show that faults formed during a second deformation phase are not necessarily orthogonal to the principal stresses of the secondary tectonic stage. Rather, they are parallel to the rift-bounding faults, indicating that the geometry inherited from the first tectonic phase acts on the orientations of new faults. Richard and Cobbold (1990) pointed out that an intact sand/silicone cake submitted to an oblique compression presents two kinds of faults: steeply-dipping, nearly pure strike-slip faults that accommodate the horizontal displacement, and shallowly-dipping, nearly pure reverse faults that accommodate the vertical displacement. The newly formed faults are perpendicular to the maximum compressive stress. In the present experiments EC 60°s and EC 60°, reverse faults are oblique to the secondary tectonic stress state but parallel to the primary normal faults, further suggesting that the geometry inherited from the first tectonic phase influences the creation of new faults and their slip direction.

Following Anderson (1951) and assuming fracturing of an homogeneous medium, σ_2 must lie within the fault plane, so slip on the fault cannot be oblique, it must be either dip-slip or strike-slip. Figs. 9 and 10 illustrate the discrepancy between the Anderson theory and optimal slip in our experiments. EE60°s, EE60°, EC 60°s and EC 60° have oblique slip. Bott (1959) explored fractures in media with inhomogeneous elastic properties and strength. He concluded that oblique-slip is possible during reactivation of a fault plane when the horizontal principal stresses lie obliquely to the strike. Experiments EE60°s, EE60°, EC 60°s and EC 60° seem to belong to this case where the horizontal principal stress lies obliquely to the strike of pre-existing faults in an ianisotropic medium.

Brun and Nalpas (1996) observe the reactivation of primary

graben bounder faults during an oblique compressive secondary tectonic phase. However, they describe a complete strain partitioning between thrust faults along the graben bounders and strike-slip faults within the graben trending oblique to the graben bounders. In contrast to them, we observe reverse faults parallel to the graben bounders partly accommodating the strike-slip movement (EC 60°s and EC 60°). Our experiments show a tendency toward strain partitioning, but not complete strain partitioning. This difference may come from our silicone/sand model that was differently built from that of Brun and Nalpas. The brittle/ductile ratio is much higher in the case of Brun and Nalpas's experiment than in ours, which may explain the differences between their results and ours. Brun and Nalpas do observe an oblique slip but in the case of an oblique inversion in a purely brittle system when the angle between the compression and extension directions of the first stage is less than 45°. The oblique slip disappears when this angle is more than 45°. In this case, normal faults are reactivated in strike-slip mode and shortening perpendicular to normal faults is only accommodated by newly formed reverse faults. In our experiment, where the angle is 60°, oblique slip is observed and could be due to a low brittle/ductile ratio.

5. Conclusions

The reactivation of a set of grabens due to a new tectonic stress field in a brittle sedimentary cover overlying a viscous salt layer has been studied by means of analogue modelling with sand and silicone putty, following Hubbert's (1937) principles. The applied secondary tectonic stress varied between compressive and extensive, and was either parallel to the primary tectonic stress or oblique (60°) to the latter.

No en échelon faults appeared during the secondary tectonic phase, whether the stress was coaxial or oblique to the primary tectonic stress. All newly formed faults were parallel to the first phase faults, indicating that geometry and orientation of pre-existing faults greatly influence the newly formed faults.

All faults formed during the primary tectonic phase were reactivated in the experiments carried out with no post-rift sedimentation. We can postulate that already existing faults were reactivated under low sedimentation rates, whereas a high sedimentation rate may favour the locking-up of some former faults. Strike-slip was observed during an oblique secondary tectonic stress state on both former and newly formed faults. All faults show oblique slip during the second tectonic stage.

In the case of an oblique secondary deformation phase, the strike-slip component is greater in grabens that have been loaded by sediments than those without. As a result, sedimentation affects the ratio of dip-slip vs. strike-slip on normal faults created during the first tectonic stage.

In experiments carried out with an oblique and exten-sional secondary deformation phase, the dip-slip component accounts for more than 50% of displacement on all normal faults.

In experiments carried out with an oblique and compressive secondary deformation phase, reverse fault slip is exactly the optimal slip expected. The reactivation of normal faults depends on the post-rift sedimentation in the grabens. Normal faults without post-rift sedimentation show mainly a reverse dip-slip reactivation, corresponding to a vertical position of σ_3, whereas normal faults with a post-rift sedimentation show mainly a strike-slip reactivation, corresponding to a vertical position of σ_2. The positions of the minor and mean principal stresses of the second tectonic stage are controlled by the occurrence of post rift sedimentation, in the experiments.

References

Anderson, E.M., 1951. The dynamics of faulting and dyke formation with applications to Britain. Olivier, Boyd (Eds.), Edinburgh, 203pp.

Bartholomew, I.D., Peters, J.M., Powell, C.M., 1993. Regional structural evolution of the North Sea: oblique-slip and reactivation of basement lineaments. In: Parker, J.R. (Ed.). Petroleum Geology of Northwest Europe: Proceedings of the 4th Conference. Geological Society London, pp. 1109–1122.

Bott, M.H.P., 1959. The mechanics of oblique slip faulting. Geological Magazine 96, 109–117.

Brace, W.F., Kohlstedt, D.L., 1980. Limits on lithospheric stress imposed by laboratory experiments. Journal of Geophysic Research 85, 6248–6252.

Brun, J.P., Nalpas, T., 1996. Graben inversion in nature and experiments. Tectonics 15, 677–687.

Byerlee, J.D., 1978. Friction of Rocks. Pageoph 116. Birkhauser Verlag, Basel.

Carter, N.L., Horseman, S.T., Russel, J.E., Handin, J., 1993. Rheology of rocksalt. Journal of Structural Geology 15, 1257–1271.

Cobbold, P.R., Bale, P., Marquer, D., Vendeville, B., 1986. Sense of wrenching in crustal flower structures. Abstract, Shear Criteria meeting, London.

Cobbold, P.R., Rossello, E., Vendeville, B., 1989. Some experiments on interacting sedimentation and deformation above salt horizons. Bulletin de la Société géologique de France 8 (3), 453–460.

Dauteil, O., Brun, J.P., 1993. Oblique rifting in a slow-spreading ridge. Nature 361, 145–148.

Davidson, I., Insley, M., Harper, M., Weston, P., Blundell, D., McClay, K., Quallington, A., 1993. Physical modelling of overburden deformation around salt diapirs. Tectonics 228, 225–274.

Davy, P., Cobbold, P.R., 1988. Indentation tectonics in nature and

experiment. 1. Experiments scaled for gravity. Bull. Geol. Inst. Uppsala, N.S. 14, 129–141.

Desrues, J., 1985. Naissance des bandes de cisaillement dans les milieux granulaires: expérience & théorie. Les instabilités mécaniques, développement et périodicité. Gratier, J.P. (Ed.), Grenoble, France.

Eisenstadt, G., Withjack, M.O., 1995. Estimating inversion: results from clay models. Basin inversion. In: Buchanan, J.G., Buchanan, P.G. (Eds.), Geological Society Special Publication 88, 119–136.

Faccenna, C., Nalpas, T., Brun, J.P., Davy, P., 1995. The influence of pre-existing thrust faults on normal fault geometry in nature and in experiments. Journal of Structural geology 17, 1139–1149.

Faerseth, R.B., 1996. Interaction between Permo-Triassic and Jurassic extensional fault-blocks during the development of the northern North Sea. Journal of the Geological Society of London 153, 931–944.

Handin, J., 1969. On the Coulomb–Mohr failure criterion. Journal of Geophysical Research 74, 22.

Hubbert, M.K., 1937. Théorie of scale models as applied to the study of geology structures. Bulletin of the Geological Society of America 48, 1459–1520.

Hubbert, M.K., 1951. Mechanical basis for certain familiar geologic structures. Bulletin of the Geological Society of America 62, 355–372.

Huyghe, P., Mugnier, J.L., 1992. Short-cut geometry during structural inversions: competition between faulting and reactivation. Bulletin de la Société Géologique de France 163, 691–700.

Keep, M., McClay, K.R., 1997. Analogue modelling of multiphase rift systems. Tectonophysics 273, 239–270.

Krantz, R.W., 1991. Measurements of friction coefficients and cohesion for faulting and fault reactivation in laboratory models using sand and sand mixtures. Tectonophysics 188, 203–207.

Letouzey, J., 1990. Fault Reactivation, Inversion and Fold-thrust Belt. Petroleum and Tectonics in Mobile Belts. Technip Edition, Paris, pp. 101–128.

Mandl, G., 1988. Mechanics of tectonic faulting. Models and basic concepts. In: Zwart H.J. (Ed.), Development in Structural Geology 1, Elsevier.

Mandl, G., DeJong, L.N.J., Maltha, A., 1977. Shear zones in granular material. Rock Mechanic 9, 95–144.

McClay, K.R., White, M.J., 1995. Analogue modelling of orthogonal and oblique rifting. Marine and Petroleum Geology 12, 137–151.

Oudmayer, B.C., Dejager, J., 1993. Fault reactivation and oblique-slip in the Southern North Sea. In: Parker, J.R. (Ed.). Petroleum Geology of Northwest Europe: Proceedings of the 4th Conference. Geological Society London, pp. 1281–1292.

Richard, P., Cobbold, P.R., 1990. Experimental insights into partitioning of fault motions in continental convergent wrench zones. Annales Tectonicae (special issue) IV, 35–44.

Richard, P., Krantz, R.W., 1991. Experiments on fault reactivation in strike-slip mode. Tectonophysics 188, 117–131.

Tron, V., Brun, J.P., 1991. Experiments on oblique rifting in brittle-ductile systems. Tectonophysics 188, 71–84.

Vendeville, B.C., Jackson, P.A., 1992. The rise of diapirs during thin-skinned extension. Marine and Petroleum Geology 9, 331–353.

Weijermars, R., 1986. Flow behaviour and physical chemistry of bouncing putties and related polymers in view of tectonic laboratory applications. Tectonophysics 124, 325–358.

Weijermars, R., Jackson, M.P.A., Vendeville, B.C., 1993. Rheological and tectonic modelling of salt provinces. Tectonophysics 217, 143–174.